Tropical Inversions near the 0°C Level

RICHARD H. JOHNSON, PAUL E. CIESIELSKI, AND KENNETH A. HART*

Department of Atmospheric Science, Colorado State University, Fort Collins, Colorado

(Manuscript received 24 April 1995, in final form 18 December 1995)

ABSTRACT

Soundings taken from the tropical western Pacific warm pool region during TOGA COARE reveal the common occurrence of temperature and moisture perturbations near the 0°C level. The perturbations frequently are characterized by shallow layers of increased stability (or occasionally temperature inversions) and reversals or inflections in the vertical profile of specific humidity. Similar temperature and moisture inversions have been observed elsewhere in the Tropics and midlatitudes but have not received much attention. Isothermal layers are known to exist just below the melting level in stratiform rain regions; however, not all stable layers observed over the warm pool are confined to precipitation systems. The perturbation in the specific humidity profile accounts for the often-observed double-peak structure in the apparent moisture sink Q_2 in the Tropics.

Stratification of the data based on relative humidity criteria indicates that the stable layers near the 0°C level generally fall into two main classifications: anomalously cool–moist conditions at and slightly below the 0°C level and anomalously warm–dry conditions at and just above. The former occur primarily within or in close proximity to precipitating systems, suggesting they are a result of the direct effects of melting. Soundings in the latter group typically occur outside convective areas. Mechanisms for formation of the warm–dry stable layers are unclear at this time, but advective, radiative, gravity wave, and melting effects may all play some role. In some cases they may simply be remnant melting layers from past convection.

There is evidence to indicate that the stable layers near the 0°C level affect tropical cloud populations. Convection impinging upon or penetrating the stable layers may detrain significantly near the 0°C level, thereby contributing to perturbations in the moisture profile there. Midlevel cloud layers that are commonly observed in the Tropics may be evidence of this detrainment.

Another primary finding is the frequent occurrence of a trade wind stable layer over the warm pool. Though not widely recognized, this finding is consistent with the prevalence of trade cumulus clouds in the western Pacific region. The trade inversions often coexist with, but are distinct from, the inversions near the 0°C level.

1. Introduction

Among the most prominent features of soundings over the tropical oceans are the sharp inversions in temperature and moisture associated with the trade wind cumulus layer, which typically lies between 1.5 and 2.5 km. Soundings from the Atlantic–Caribbean region reveal the marked stability of the trade inversion and its pronounced annual variability [Fig. 1a, a 10-yr climatology of the temperature lapse rate at 50-mb resolution taken from the West Indies data of Jordan (1958)]. During the winter months, when precipitation is low, the trade inversion is strongest (Gutnick 1958).[1] During the summer, the inversion weakens and rises slightly, as also noted by Gutnick.

The primary focus of this study is on yet another feature of Fig. 1a, a layer of increased stability near the 0°C level (~600 mb or 4 km) during the summer months. This stable layer, though shallow, is only slightly weaker than the trade stable layer during the summer. A similar analysis, but with a higher vertical resolution (25 mb), based on sounding data from the western Pacific warm pool obtained during the four-month TOGA COARE (Tropical Ocean–Global Atmosphere Coupled Ocean–Atmosphere Response Experiment; Webster and Lukas 1992) corroborate the Atlantic results: stable layers of comparable magnitude can be seen near both the trade inversion (800 mb) and 0°C level (Fig. 1b). These results are based on an objective analysis of sounding data (daily values at 0000

* Current affiliation: Air Force Global Weather Central, Offutt AFB, Nebraska.

Corresponding author address: Dr. Richard H. Johnson, Department of Atmospheric Science, Colorado State University, Fort Collins, CO 80523.
E-mail: rhj@vortex.atmos.colostate.edu

[1] The analysis in Fig. 1 does not indicate the presence of actual temperature inversions ($dT/dz > 0$) because of the coarse vertical resolution of Jordan's (1958) tabulated data. The study of Gutnick (1958), however, shows that temperature inversions at the top of the trade wind layer are common throughout the West Indies region, particularly during the winter months.

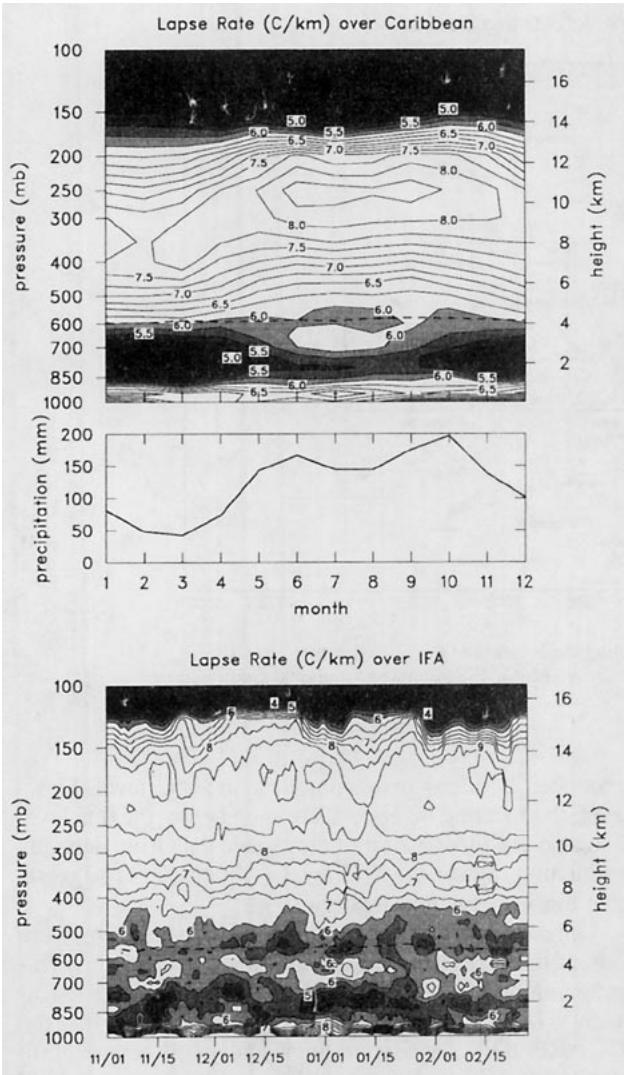

FIG. 1. (a) Annual cycle of temperature lapse rate (top panel) computed from the ten-year climatology of West Indies data from Jordan (1958). Shaded contours indicate regions of greater stability with a contour interval of 1°C km^{-1}. Dashed line indicates 0°C level. Annual cycle of precipitation (bottom panel) based on climatological data for West Indies stations used by Jordan (1958): Miami, Florida; San Juan, Puerto Rico; and Swan Islands. (b) Time series from 1 November 1992 to 28 February 1993 of temperature lapse rate computed by averaging 25-mb gridded data (1° horizontal resolution) over the COARE Intensive Flux Array. Shaded contours indicate regions of greater stability with a contour interval of 1°C km^{-1}. Dashed line indicates 0°C level.

UTC) over a small area at the center of the COARE domain, the Intensive Flux Array (IFA) centered at 2°S (Fig. 2). Similar stable layers near the 0°C level have been reported in the tropical eastern Pacific by Haraguchi (1968), where they were attributed to large-scale subsidence in the subtropical high, and over India by Ananthakrishnan and Keshvamurthy (1974).

TOGA COARE data also indicate the common occurrence of tradelike stable layers near 800 mb or 2 km over the western Pacific warm pool (Fig. 1b). Firestone and Albrecht (1986), Kloesel and Albrecht (1989), and Schubert et al. (1995) have reported similar trade wind stable layers near 2 km extending all the way to the equator in the eastern Pacific and Atlantic. The fact that such layers exist in the equatorial western Pacific (not just the trade wind belts) has not been widely recognized (Schubert et al. 1995).

In addition to the frequent stable layers near 0°C, the sounding data often reveal corresponding reversals in the specific humidity (q) gradient near the same level [similar to the "q reversals" of Betts and Albrecht (1987) for the trade inversion, but at a higher level]. Climatologies of tropical relative humidity support these findings (Liu et al. 1991; Gutzler 1993), as well as the recent COARE study of Mapes and Zuidema (1996, hereafter referred to as MZ96). The inversions in q near 0°C and at other levels may be associated with dry intrusions from the subtropics discussed by Parsons et al. (1994), Numaguti et al. (1995), Yoneyama and Fujitani (1995), and MZ96.

Since the 0°C stable layers in Fig. 1 frequently occur during periods of heavy rainfall, they may in part be a direct manifestation of melting in precipitation systems, which tends to produce an isothermal layer several hundred meters deep just below the melting level (Findeisen 1940; Wexler et al. 1954; Atlas et al. 1969; Riehl 1977; Stewart et al. 1984; Willis and Heymsfield 1989). Indeed, many soundings exhibit direct melting-layer signatures. UHF wind profiler data show the prominence of the melting layer in the COARE region, even when precipitation did not reach the ground (Gage et al. 1994; Williams et al. 1995). However, observations of stable layers at great distances from convection and in very dry environments suggest other mechanisms may be involved in their formation, although some of these cases may simply be remnant stable layers from melting in previous convection. One promising alternative explanation involves the longwave–radiative stabilization of "dry tongues" associated with dry intrusions from the subtropics (MZ96).

The purpose of this paper is to document the characteristics of temperature and moisture perturbations near the 0°C level using TOGA COARE sounding data over the western Pacific warm pool. Mean thermodynamic profiles are presented in section 3. Next, in section 4, a stratification of the data by midtropospheric relative humidity is introduced. Possible causal mechanisms for the inversions will be briefly discussed in section 5. In section 6 it will be shown that the temperature and moisture perturbations near the 0°C level are prevalent enough to influence vertical distributions of latent heating and moistening over the warm pool. Finally, potential impacts on tropical cloud populations will be explored in section 7.

2. Data analysis and procedures

During the TOGA COARE Intensive Observing Period (IOP, November 1992–February 1993), a net-

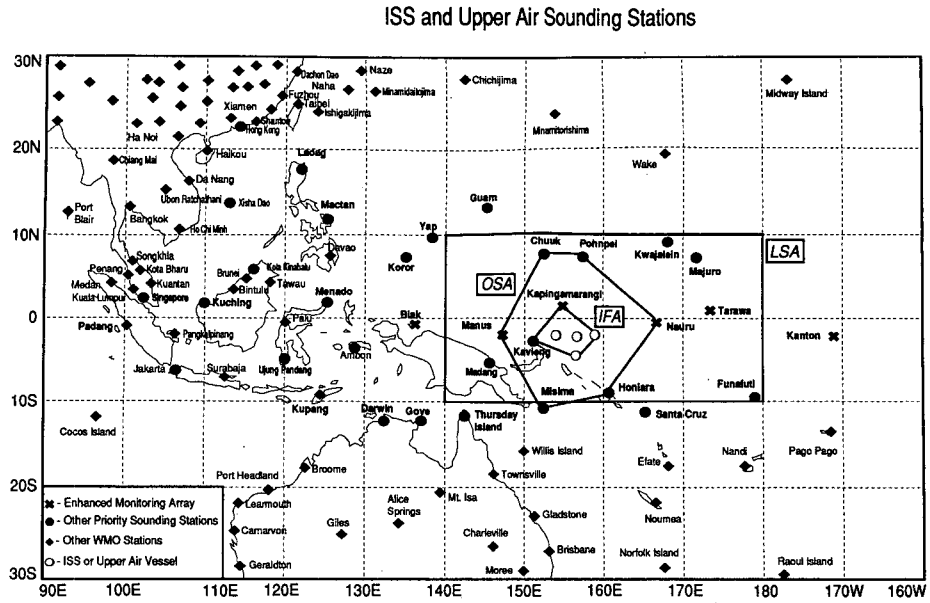

FIG. 2. The TOGA COARE sounding network showing the location of the intensive flux array (IFA), the outer sounding array (OSA), and the large-scale array (LSA). ISS refers to Integrated Sounding System (Parsons et al. 1994).

work of sounding stations was established over the equatorial western Pacific to determine the mesoscale to synoptic-scale structure of atmospheric circulation systems over the warm pool region. The network (Fig. 2) consisted of nested arrays, ranging from the synoptic scale (the large scale array or LSA, with twice per day soundings), to the subsynoptic and mesoscale (the outer soundings array or OSA and the intensive flux array or IFA, both with four per day soundings). Instrumentation included NCAR (National Center for Atmospheric Research)/NOAA (National Oceanic and Atmospheric Administration) Integrated Sounding Systems or ISSs consisting of 915-Mhz wind profilers, RASS (Radio Acoustic Sounding Systems), omegasondes (where 5-mb vertical resolution thermodynamic data have been used) and surface PAM stations (Parsons et al. 1994). In addition, there were supplemental upper-air soundings on islands and ships and upgrades to current World Meteorological Organization upper-air stations.

The bulk of the soundings used in this study employed the Vaisala H-Humicap humidity sensor. Since primary attention will be focused on atmospheric structures in the vicinity of the 0°C level, there was some concern that perturbations to the moisture profile may have arisen due to misinterpretation of the instrument calibration. However, it was determined that the humidity sensor was calibrated with respect to liquid water at all temperatures, as assumed in all processing algorithms, such that perturbations observed near the 0°C level can be assumed to be real. A second concern was that condensation and subsequent freezing on the temperature sensor could have produced fictitious inversions near the 0°C level. However, the fact that inversions are seen below the 0°C level and also in COARE aircraft dropsonde data from descents originating above the 0°C level (Miller 1993) suggests that this effect is not important.

Unless stated otherwise, results to be shown were computed using soundings from the four ISS sites Kapingamarangi (hereafter referred to as Kapinga), Kavieng, Manus, and Nauru. At these sites during the COARE IOP, 1866 soundings had good temperature data and 1745 had good moisture data between 1000 and 400 mb.

Digitized infrared (IR) Japanese GMS-4 satellite data at 10-km horizontal resolution were provided by T. Nakazawa.

3. Mean temperature and moisture stratification

Inspection of individual soundings reveals the common occurrence of temperature T and specific humidity q perturbations near the 0°C level. However, because of their variability in the vertical and the large range of T and q in the troposphere, the perturbations are almost indiscernible in IOP-mean, tropospheric profiles of T and q (Figs. 3a and 3c). However, the derivatives of these fields with respect to height z and pressure p, dT/dz and dq/dp, do reveal local maxima at and just above the 0°C level (Figs. 3b and 3d).[2] Similar perturbations

[2] The derivative of q is shown here with respect to p because this quantity is used in (2) (section 6) to compute the apparent moisture sink Q_2.

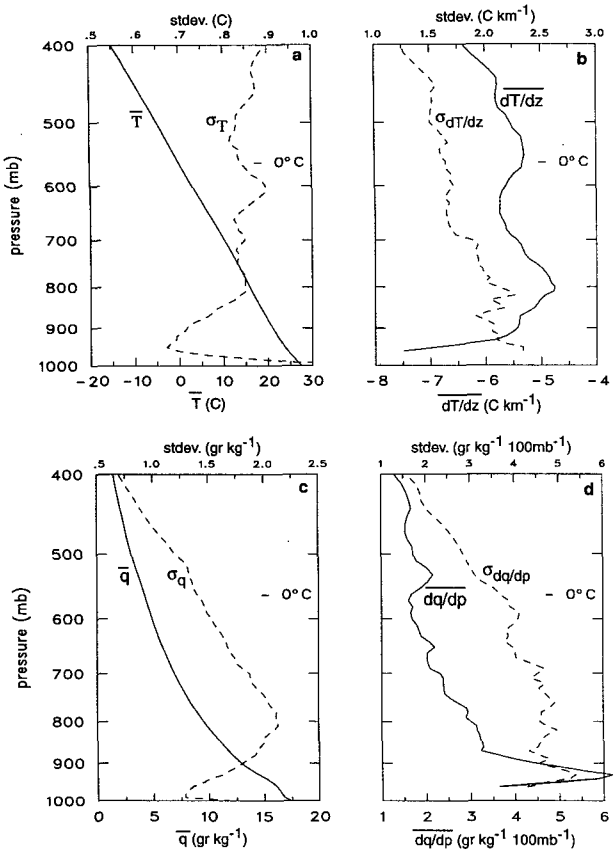

FIG. 3. Means (solid) and standard deviations (dashed) for (a) temperature (°C), (b) vertical temperature gradient (°C km^{-1}), (c) specific humidity (g kg^{-1}), and (d) vertical gradient of specific humidity (g kg^{-1} 100 mb^{-1}), computed from sounding data for four ISS sites.

near 0°C are detectable in mean sounding data for the Australian Monsoon Experiment (Mapes and Houze 1992, their Fig. 10). In the case of dT/dz, there is also a maximum near 800 mb related to the trade inversion, as has also been noted near the equator by Firestone and Albrecht (1986), Kloesel and Albrecht (1989), and Schubert et al. (1995). There is also a large peak in dq/dp near 930 mb, reflecting drying just above the mixed layer. Standard deviations of T exhibit a maximum just below the 0°C level (Fig. 3a, note change of scale) and for both T and q maxima near 800 mb (Figs. 3a and 3c), indicating large variability associated with the trade inversion [although the peak in the standard deviation of q virtually disappears when it is plotted as a fraction of the mean q at each level (MZ96, their Fig. 4)].

A convenient way of viewing the frequency distribution of stability (dT/dz) is by the use of a contoured frequency by altitude diagram (CFAD, Yuter and Houze 1995). A CFAD for stability (computed over 20-mb layers using 10-mb data) at Kapingamarangi is shown in Fig. 4 (differing only slightly from CFADs for Kavieng, Manus, and Nauru). Maxima in stability (indicated by contour ridges for $dT/dz > -5$°C km^{-1}) are evident in layers centered near three levels: 925, 800, and 550 mb. The peak near 925 mb represents the inversion atop the mixed layer, the latter manifested by the frequent occurrence of nearly dry-adiabatic lapse rates in the lowest 50 mb. The maximum near 800 mb is related to the trade inversion; however, an actual temperature inversion occurs there only ~5% of the time, unlike the trade wind belt (away from the equator) where strong inversions are the normal state of affairs (e.g., Gutnick 1958; Augstein et al. 1974). Finally, an increase in the number of stable layers (as well as a decrease in the number of unstable layers) can be seen near the 0°C level, although no single, well-defined peak is present.

Frequency distributions of temperature lapse rates exceeding certain thresholds, obtained by integrating the stability CFADs (using thresholds for dT/dz of −3°, −4°, and −5°C km^{-1}), are shown in Fig. 5. From Fig. 4 it is evident that a lapse rate of 5°C km^{-1} is about 1°C km^{-1} less than the median between 900 and 500 mb and hence represents relatively stable conditions. The results for Kapinga, Kavieng, Manus, and Nauru indicate that while stable layers appear to be common throughout the troposphere, two prominent maxima occur at each site: one near 800 mb associated with the trade inversion and a slightly weaker maximum between 500 and 600 mb or near the 0°C level.[3] These profiles very closely resemble the distributions of sharp relative humidity decreases with height presented by MZ96 (their Fig. 6), suggesting a close relationship between temperature and moisture perturbations. The upper maximum in Fig. 5 exhibits a double-peak structure near 0°C at three of the four sites, one peak at or just below 0°C and another near 520 mb. For the more stable thresholds ($dT/dz = -4$° and −3°C km^{-1}), the 0°C maximum becomes progressively less prominent relative to the trade-layer peak.

The results in Fig. 5 are based on frequency of occurrence in 10-mb layers. For this depth and a lapse-rate threshold of 5°C km^{-1}, over 50% of the soundings taken at these four sites during COARE exhibited trade-wind-type stable layers and over 40% stable layers near the melting level. However, the use of 10-mb layers underestimates the true number of inversions associated with the trade and 0°C levels. For example, if we select 100-mb layers centered at 800 and 560 mb, corresponding to the trade and 0°C layers, the mean frequency of occurrence of stable layers with the 5°C km^{-1} threshold is 82% and 60%, respectively.

Two important conclusions emerge.

[3] There is also a minor peak marking the inversion atop the mixed layer near 925 mb. However, this peak is not present at Kavieng, presumably due to the much larger diurnal variation of the mixed layer at this land-dominated site.

• *First, the trade inversion (or stable layer) appears to be a common phenomenon throughout the Tropics, even along the equator within the heavily raining ITCZ region over the warm pool.* Though not widely recognized, this finding is consistent with the central and eastern Pacific studies of Firestone and Albrecht (1986), Kloesel and Albrecht (1989), and Schubert et al. (1995), as well as the frequent observations of trade cumulus-type clouds over the warm pool. An example is shown in Fig. 6, a photograph taken from the R/V *Vickers* at 2.1°S, 156.3°E during November 1992. In addition to the numerous shallow cumulus, there is also a precipitating cumulus congestus in this photograph extending to about 5 km (assuming a cloud base of ~0.5 km). These cloud types typically exist during the suppressed phase of the intraseasonal or Madden–Julian oscillation (MJO) or within the regions of subsiding air between deep convective cores within the ITCZ (e.g., Kloesel and Albrecht 1989; Sun and Lindzen 1993).

• *Second, stable layers near the melting level are a very common phenomenon over the warm pool.* More than one-half of the soundings contained recognizable stable layers within an ~100 mb layer centered near the 0°C level. Since only a small fraction of the balloons ascended into precipitating systems (12% of the soundings had precipitation within one hour of launch time), many of these stable layers occurred outside them.

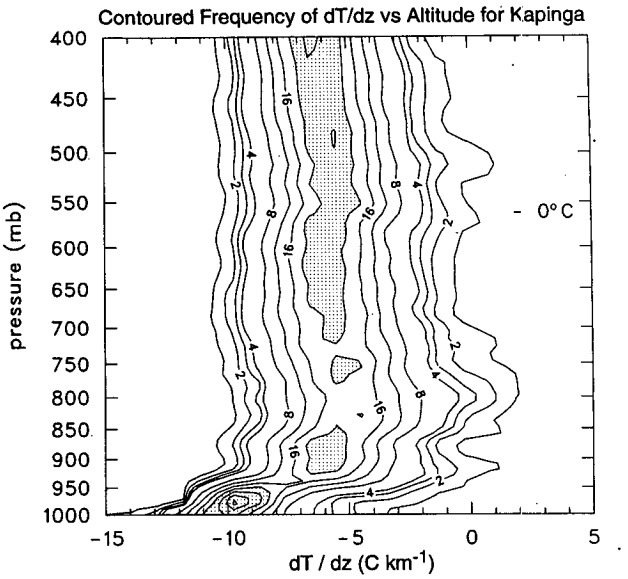

FIG. 4. Contoured frequency by altitude diagram for stability (dT/dz) at Kapinga computed using centered differences over 20 mb on 475 soundings from the COARE IOP. Isolines represent the frequency (percent) of observations, at a particular level, which have stabilities in a 1°C km^{-1} sized bin; note that the contour interval is 1% for low frequencies and 4% for frequencies higher than 4%. Frequencies higher than 20% are shaded.

The IFA time series in Fig. 1b indicates that the trade- and melting-level stable layers are common over the warm pool, although there are periods when they are disrupted. For example, the time series of stability (dT/dz) at Kapinga shown in Fig. 7 indicates fluctuating but persistent stable layers near 800 mb and the 0°C level for most of the December–January period. The stable layers near the 0°C level appear to last a day or less, but actual lifetimes are ambiguous from a time series at a single location. Nevertheless, on some occasions (e.g., the end of January) the stable layers appear to persist for several days. Some disruption in this pattern occurred during a short period centered around 1 January. This period corresponds to the time of a strong westerly wind burst (Gutzler et al. 1994), as indicated by the accompanying time series of the 700-mb wind. During the westerly burst, the lower troposphere was extremely dry. A time series of q' (specific humidity deviation from the mean) illustrates the drying, which eventually descended to near the surface in early January. Similar drying episodes, attributed to intrusions from subtropical latitudes, have been reported during other periods in the IOP (Numaguti et al. 1995; Yoneyama and Fujitani 1995; MZ96). These authors report descent of dry layers at ~400 m day^{-1}, roughly equivalent to the subsidence rate required to offset radiative cooling. Figure 7 also shows descent of stable layers near the 0°C level at similar rates. The maximum lower-tropospheric moistening and precipitation preceded the maximum westerlies by a week to ten days, consistent with the findings of Hendon and Liebmann (1990) in a study of the 30–50 day oscillation at Darwin and the COARE-IOP results reported by Nakazawa (1995). MZ96 have shown that the dry layers typically have a positive virtual temperature anomaly near their bases, leading them to propose that longwave radiation may be acting on dry tongues to produce the stable layers.

The profile of dq/dp (Fig. 3d) indicates a local minimum in the lapse of q near 0°C. Consistent with this minimum is a peak in the percentage of soundings exhibiting inversions in q ($dq/dp < 0$) at this level (Fig. 8). However, unlike dT/dz (Fig. 4), dq/dp does not have a peak near the trade inversion level. Previous studies (Augstein et al. 1974; Betts and Albrecht 1987) have shown that off the equator in the Atlantic and eastern Pacific inversions in q are commonplace atop the trade cumulus layer. Evidently, although trade stable layers are present along the equator over the warm pool, they are much weaker and actual q inversions occur less than about one-quarter of the time. The sharp minimum at 930 mb is related to strong drying atop the mixed layer.

The temperature and moisture perturbations correspond to a local maximum in relative humidity (RH) near the 0°C level, as can be seen in the mean RH profile (Fig. 9, dashed curve, values for $T < 0$°C com-

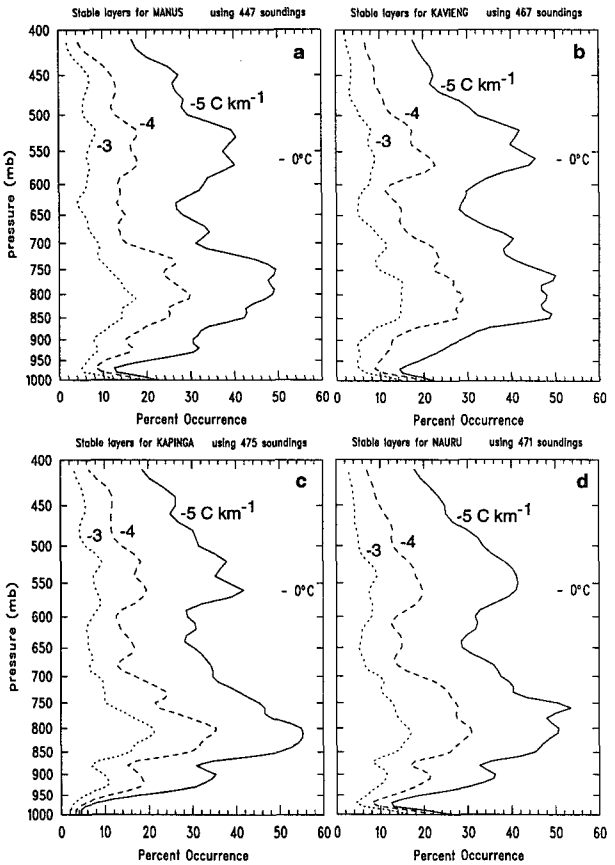

FIG. 5. Cumulative frequency (percent) of stability (dT/dz) greater than $-5°$ (solid), $-4°$ (dashed), and $-3°C\ km^{-1}$ (dotted) for (a) Manus, (b) Kavieng, (c) Kapinga, and (d) Nauru. These profiles were generated by integrating, at each vertical level, the percentages in each stability bin of the CFADs (such as in Fig. 4) to the right of the specified stability criterion.

puted with respect to ice and liquid water). The maximum near 0°C is most prominent in the liquid water case and that profile compares well with the findings of Liu et al. (1991) and Gutzler (1993). Figure 9 also contains a CFAD for RH (with respect to ice for $T < 0°C$), which reveals an interesting behavior: at low levels, the mean and the most frequently occurring RH coincide, while at higher levels, the two increasingly diverge. The frequent occurrence of high RH at higher levels indicates mid- to upper-tropospheric clouds are common over the warm pool, but there are also a considerable number of cases with quite dry conditions there, which reduces the mean RH. In contrast, very dry conditions at the surface (RH < 50%) are virtually nonexistent in this region. This behavior is reflected in the standard deviation of RH, which steadily increases with height through the troposphere (Fig. 9).

4. Classification of stable layers

The preceding section established that stable layers near the 0°C level are nearly as common as trade wind stable layers over the warm pool. In addition, a broad maximum in q inversions is found centered just below the 0°C level with a local maximum in relative humidity near 0°C. A relationship between stable layers and q perturbations near the 0°C level can be seen in Fig. 10, a plot of the difference in q between the cases when stable layers exist within 50 mb of the 0°C level and when they do not for three lapse-rate thresholds (3°, 4°, and $5°C\ km^{-1}$), involving 11%, 24%, and 60% of the soundings, respectively. For lapse rate thresholds of 4° and $5°C\ km^{-1}$, soundings with stable layers are moister at and below the 0°C level, suggesting many stable layers are associated with melting. There is a sharp falloff of moisture centered around 0°C for all stability thresholds, supporting the idea of MZ96 that radiative stabilization may be contributing to the formation of many of the stable layers.

In an attempt to understand the causes of the T and q perturbations, a stratification of the data is sought that exploits what is already known about one process that produces stable layers, namely, melting. Soundings exhibiting melting layers, such as the one for Kapinga at 1800 UTC 5 November (Fig. 11), are typically characterized by very moist conditions throughout much of the troposphere. An exception is the situation where the lower troposphere is influenced by mesoscale unsaturated downdrafts, yielding "onion"-type profiles, as described by Zipser (1977). Such soundings, although observed, were rather rare during COARE, however.

Since clouds and precipitation are known to be associated with melting-produced stable layers, relative humidity is selected as a criterion for stratifying the soundings. In order to best reflect the presence of clouds, RH with respect to ice is used above the 0°C level. From Fig. 9 it is seen that the standard deviation of RH (σ_{RH}) is small in the boundary layer and increases upward, becoming quite large in the upper troposphere.

To subdivide the soundings, the average RH (RH_{ave}) in the 400–700-mb layer for soundings having lapse rates less than $5°C\ km^{-1}$ over a 20-mb-deep layer within 50 mb of the 0°C level is compared to the time-mean RH ($\overline{RH}$) for that layer. The 400–700-mb layer is chosen because above 400 mb the sounding data are sometimes missing and moisture data are less reliable, while below 700 mb drying from unsaturated downdrafts can occur (results based on the selection of a 400–1000-mb average are qualitatively the same). Based on 400–700-mb layer means and standard deviations for each of the four sites (58 ± 23%, 64 ± 23%, 66 ± 22%, and 60 ± 21% for Kapinga, Nauru, Kavieng, and Manus, respectively), four RH thresholds were established: very moist (RH++), moist (RH+), dry (RH−), and very dry (RH−−); representing $RH_{ave} > \overline{RH} + \sigma_{RH}$, $\overline{RH} < RH_{ave} < \overline{RH} + \sigma_{RH}$, $\overline{RH} - \sigma_{RH} < RH_{ave} < \overline{RH}$, and $RH_{ave} < \overline{RH} - \sigma_{RH}$, respectively.

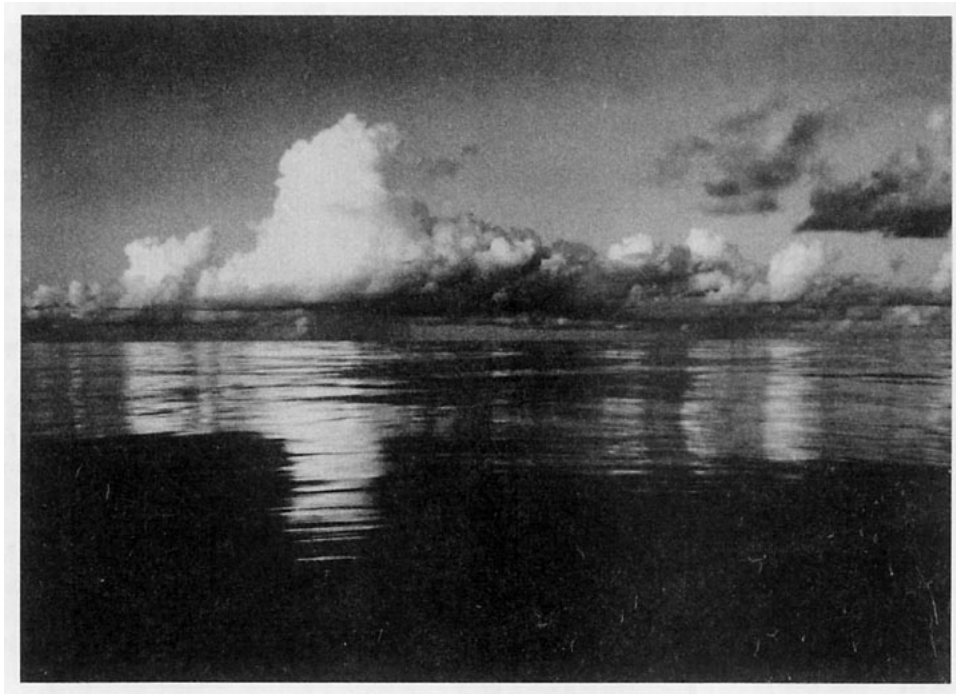

FIG. 6. A photograph taken from the R/V *Vickers* (2.1°S, 156.3°E) during November 1992 (courtesy C. DeMott). The photograph shows numerous shallow cumulus in addition to a precipitating cumulus congestus with its top near 5 km.

Profiles of q' and T' (deviation from the IOP mean) corresponding to these four categories are shown in Fig. 12. The four groupings of soundings in Fig. 12 containing stable layers near the 0°C level represent 60% (1047) of all 1745 IOP soundings for the four sites.[4] The individual categories, from moistest ($RH_{ave} \geq 80\%-90\%$) to driest ($RH_{ave} \leq 35-45\%$), constitute 11%, 43%, 32%, and 14%, respectively, of these 1047 stable-layer soundings. Thus, assuming RH $\geq$ 80%–90% between 700 and 400 mb is a good indicator of precipitation, 7% (or 11% of 60%) of all soundings at the four sites during the IOP had stable layers that are presumably directly attributable to ascents through precipitation.

Broadly, we see from Fig. 12 that warm cases are dry and cool cases are moist—largely because most of the rainy areas are cooled by evaporation and melting, and few, if any, soundings ascend into warm, moist updraft cores. Figure 12a shows that the RH++ cases are 1–2 g kg^{-1} moister than the mean in the midtroposphere and have a negative T' peak between 600 and 700 mb (Fig. 12b), presumably associated with the direct effects of melting and evaporation. Because soundings were selected for stable layers at least 20 mb deep within 50 mb of the 0°C level, the profiles of T' in Fig. 12b tend to show a positive slope near 0°C. This stable layer shifts to higher levels for drier cases, a point that will be discussed further in connection with Fig. 17 below. In sharp contrast, the driest cases producing stable layers near the melting level are characterized by a prominent warm anomaly above 0°C.[5] The intervening categories have T' profiles intermediate to the two extremes; however, the RH+ category still has a prominent melting/cooling peak ($T' < 0$ near 600 mb), while the moderately dry category has a complicated structure with two T' maxima above and below 0°C. The very cool, moist surface conditions for RH++ support the association of these cases with precipitating convection.

To determine possible diurnal influences to the RH-stratified profiles in Fig. 12, diurnal variations of RH, T, and q have been computed and are shown as deviations from daily means in Fig. 13. Above 850 mb,

[4] Soundings that terminated before 400 mb or had missing RH data below that level were excluded from the analysis. Since soundings that ascend into precipitation often terminate just above the 0°C level due to icing, there may be a slight bias in our sample against "precipitating" soundings.

[5] Mapes and Zuidema (1996) note that the tropospheric mean T varies on the timescale of the 30–60-day oscillation with prominent warm anomalies in December and mid- to late January. The driest (RH−−) cases tend to be favored around these times (see Fig. 15), indicating that at least some of the deep-layer warming for RH−− in Fig. 12b can be attributed to low-frequency variability.

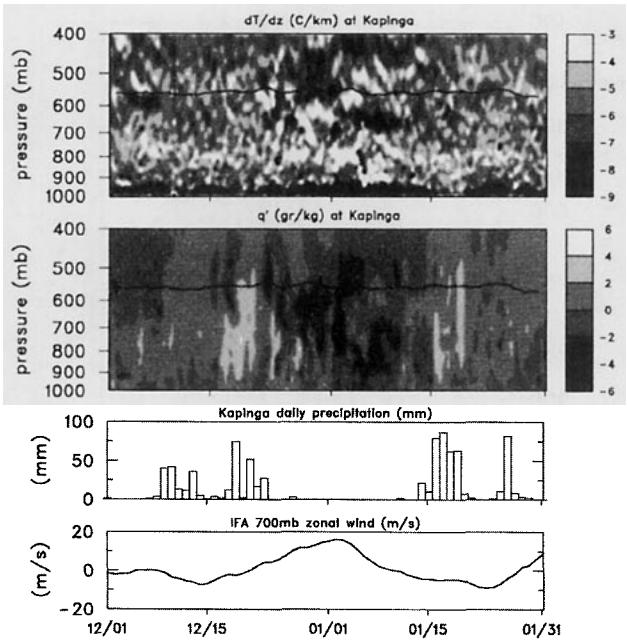

FIG. 7. Time series from 1 December 1992 to 31 January 1993 of stability (°C km^{-1}), perturbation specific humidity (g kg^{-1}), and daily precipitation (mm) at Kapinga (in top three panels, respectively) and 700-mb zonal wind averaged over the IFA (bottom panel). The fields in the top two panels were constructed using 6-h, 5-mb resolution sounding data. The q' field represents a deviation from the IOP mean q at Kapinga. In the top two panels the shading convention depicts more (less) stable and moist (dry) periods in lighter (darker) shades, whereas the solid line shows the location of the 0°C level.

nighttime soundings are moister than daytime by up to 8% at 400 mb (Fig. 13a). There are at least two explanations for this behavior: 1) radiative heating of the temperature sensor and/or shortwave absorption in the upper troposphere (Randall et al. 1991) contributing to daytime upper-tropospheric warming up to 0.5°C (Fig. 13b; similar to MZ96's Fig. 8a) and/or 2) a nighttime maximum in deep convection and upper-tropospheric clouds during COARE (Chen et al. 1996). The existence of a nighttime maximum of precipitation is supported by a minimum in q (derived from the measured RH and T) at 1000 LST (Fig. 13c). Since RH− − daytime cases are favored over nighttime cases by a margin of 3 to 2, there may be a diurnally produced 700–400-mb layer mean RH bias of up to 3%–4%. However, this diurnal effect is not large enough to shift any one sounding by more than one RH category since the categories are separated by RH increments of ~22%. Conversely, RH++ nighttime cases are favored over daytime cases by roughly the same 3:2 margin.

Mean skew T plots for the four RH categories are shown in Fig. 14. The composites for the two moist cases are slightly reminiscent of Zipser's (1977) onion profile, with the suggestion of a deep cloud layer above 0°C and relatively dry conditions in the lower troposphere. The dry cases tend to be progressively drier up to about 0°C (see also Fig. 12), particularly for RH− −. They also have discernible trade stable layers near 800 mb (with corresponding drying above), especially for the driest category where a cool anomaly appears near 900 mb (Fig. 12).

The timing of the moistest and driest categories relative to the phase of the MJO is illustrated in Fig. 15, where their occurrences at the longitudes of the four sites Kapinga, Kavieng, Manus, and Nauru are indicated in a Hovmöller diagram of the outgoing longwave radiation (OLR) for the COARE intensive observing period. Not surprisingly, the moist cases preferentially occur during periods of enhanced deep convection in the active phase of the MJO, whereas the dry cases tend to be favored in between.

Composite maps of average IR temperature (a proxy for clouds) for four RH categories at Kapinga are shown in Fig. 16 (results at other sites are similar). For the driest category (RH− −), there was a local minimum of cloudiness near Kapinga, with east–west bands of clouds 5° north and south of the station (Fig. 16, top). However, the northern band has a break in it directly north of Kapinga, suggesting the possible role of dry intrusions from the subtropics. The RH− category has a more pronounced double ITCZ-type structure with a more prominent cloud minimum near Kapinga than in the RH− − case. The lack of such a prominent cloud minimum for RH− − may be due to the occurrence of many of these cases during 1–5 January (Fig. 15) when there was considerable cirrus over the

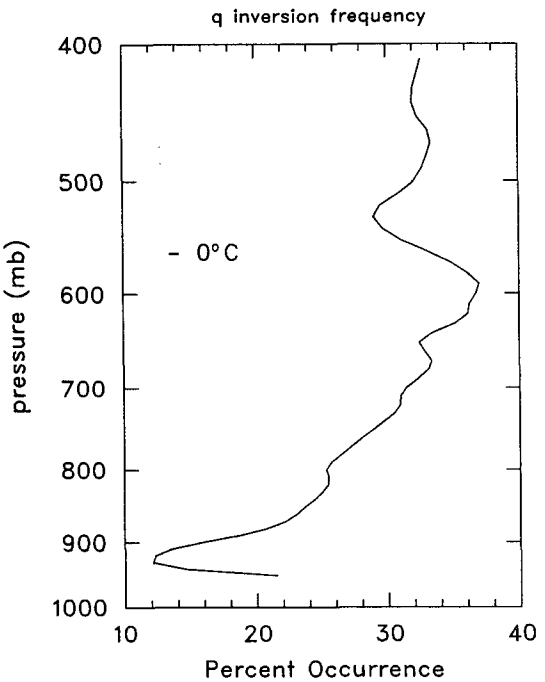

FIG. 8. Cumulative frequency (percent) of specific humidity inversions (i.e., $dq/dp \leq 0$) for four ISS sites.

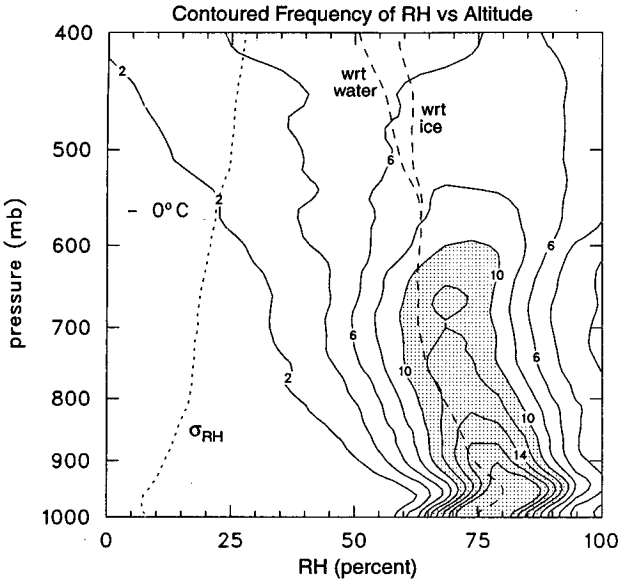

FIG. 9. Contoured frequency by altitude diagram for relative humidity with respect to ice for four ISS sites. Isolines represent the frequency (percent) of observations, at a particular level, which have values in a 5% sized bin. The contour interval is 2% with values greater than 10% shaded. Dashed curves represent the IOP-mean relative humidity computed with respect to water and ice. Dotted curve represent the IOP standard deviation of relative humidity (σ_{RH}) with respect to ice.

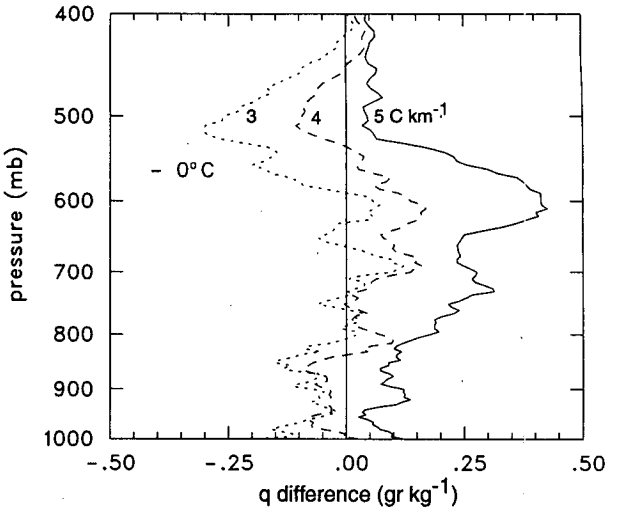

FIG. 10. Specific humidity difference (g kg^{-1}) between soundings from four ISS sites that have stable layers (using different temperature lapse rate thresholds over a depth of at least 20 mb) within 50 mb of the 0°C level and those that do not. Dotted, dashed, and solid lines were computed using 3°, 4°, and 5°C km^{-1} thresholds, respectively.

IFA associated with the westerly wind burst event. At the other extreme, stable layers under the moistest conditions occurred when there was a maximum of convection over Kapinga with bands of cold cloud tops extending eastward and to the west and southwest (Fig. 16, bottom). The RH+ category has a cloudiness pattern approximately intermediate to the two adjacent categories.

To examine the occurrences of stable layers at *any* level under different relative humidity conditions, frequency distributions of stable layers (-5°C km^{-1} threshold) for the four RH categories for all IOP soundings are presented in Fig. 17 (essentially a decomposition of the solid curves in Fig. 5). In Fig. 17 the frequencies in each category have been normalized by the peak values, which occur at the trade inversion level for all but RH++. There is a strong preference for stable layers to occur near 0°C when it is moist (RH++ and RH+), while the peak for the driest category (RH−−) is ~50 mb above the 0°C level. In other words, the peaks right at 0°C in Fig. 5 appear to be attributable to direct melting effects in precipitation systems, whereas the upper peak is associated with dry conditions aloft, suggesting a possible role of radiative stabilization in those cases (MZ96). Of course, radiation can affect all cases of strong moisture gradients; however, under moist conditions the effects are less certain owing to complications by clouds.

5. Possible mechanisms for the inversions

In the following discussion, we refer to the moist categories (RH++ and RH+) as cool–moist and the dry categories (RH−− and RH−) as warm–dry based on Fig. 12.

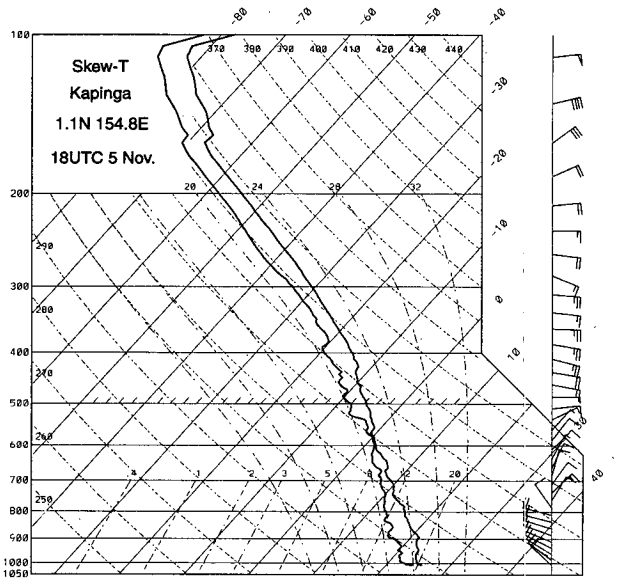

FIG. 11. Skew T diagram for Kapinga at 1800 UTC 5 November 1992 exhibiting characteristics commonly associated with the effects of melting (i.e., a shallow, cool saturated layer directly below the 0°C level).

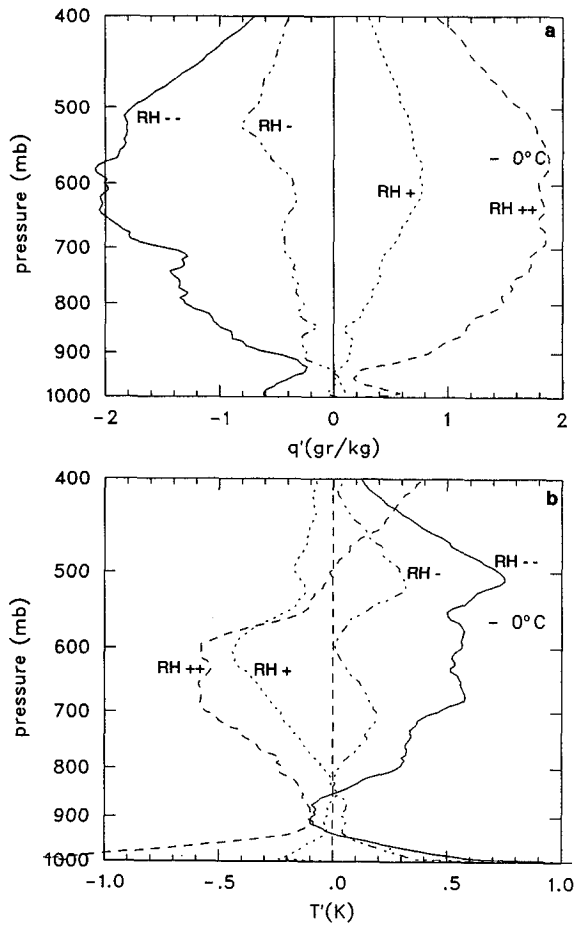

FIG. 12. Composite profiles for four ISS sites of perturbation specific humidity (q deviation from IOP mean—top panel) and perturbation temperature (T deviation from IOP mean—bottom panel) for soundings with stable layers (lapse rates $\leq$ 5°C km^{-1} over a depth of at least 20 mb) within 50 mb of the 0°C level for four RH categories described in text.

a. *Cool–moist cases*

This type is presumably associated with the direct effects of melting, either within precipitation systems (Findeisen 1940) or immediately following their decay. Once generated, the inversions may persist for periods up to a day or longer if vertical mixing or radiation does not quickly destroy them. The generally low IR-brightness temperatures associated with these cases (Fig. 16) support the direct-melting effect explanation for the cool–moist stable layers (recognizing, however, that IR-brightness temperatures and precipitation or melting are not necessarily well correlated at fine scales). Evidence for melting is also seen in the hourly rainfall data from the four sites, which indicate significant percentages of the RH++ and RH+ cases had rainfall within one hour of radiosonde launch time.

b. *Warm–dry cases*

Among the processes that may be involved in these cases are advection, radiation, and internal gravity waves, although here too some of the cases may be associated with remnant melting layers. To illustrate the possible role advection may play, a sequence of soundings at Nauru over a 2-day period is shown in Fig. 18. At 1200 UTC 16 December, the atmosphere is quite moist throughout the entire troposphere. Just six hours later, there is a sudden drying and warming over a 75-mb deep layer between 600 and 500 mb. Over the next two days, the drying extends over a much deeper layer. Mapes and Zuidema (1996) demonstrate that such intense drying cannot be explained by adiabatic vertical displacements, rather it must be accounted for by horizontal advection. Within the layer of drying, there is a concurrent surge in the northeasterly flow. Soundings from stations northeast of Nauru (Majuro and Kwajalein) show extremely dry conditions in the midtroposphere at this time. Apparently this drying is associated with an intrusion of dry air from more subtropical latitudes (Hendon and Liebmann 1990; Parsons et al. 1994; Numaguti et al. 1995; Yoneyama and Fujitani 1995; MZ96). Stable layers produced in very dry regimes, presumably connected with dry intrusions, have a peak occurrence about 50 mb above 0°C, as seen in Fig. 17. Most likely this accounts for the upper peaks in the broad maxima in stable layers near 0°C at Manus, Kavieng, and Kapinga (Fig. 5).

As previously discussed, MZ96 have shown that a sharp, dry layer (of the type illustrated in Fig. 18) can produce a strong vertical gradient in longwave radiative heating (cooling below its base and perturbation warm-

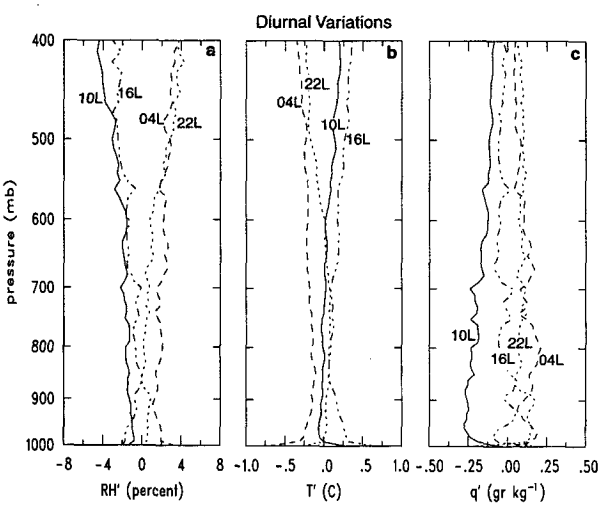

FIG. 13. Diurnal variation of (a) relative humidity (%), (b) temperature (°C), and (c) specific humidity (g kg^{-1}) presented as deviations from a daily IOP mean for four ISS sites. Dashed curves are for 0400 LST, solid for 1000 LST, dashed-dotted for 1600 LST, and dotted for 2200 LST.

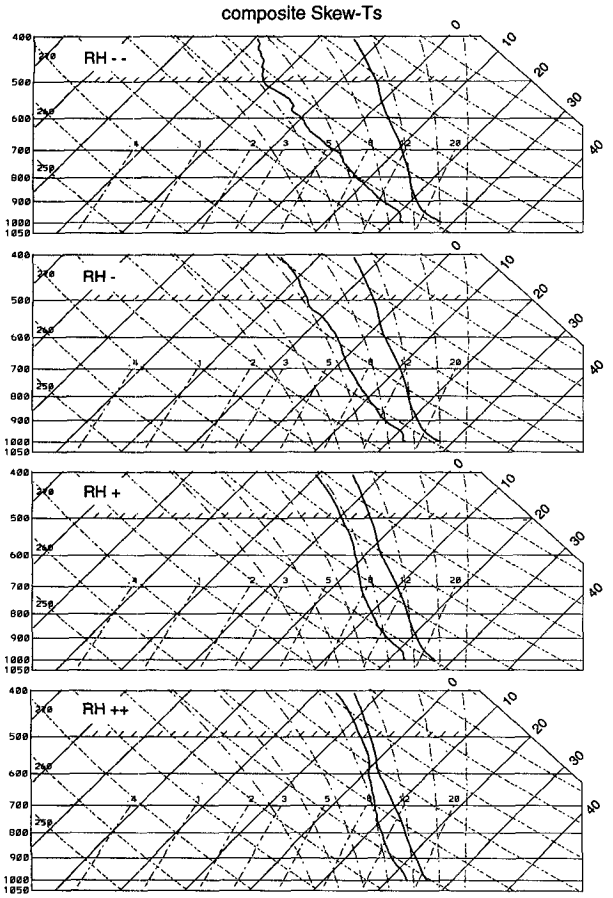

FIG. 14. Composite profiles on skew T diagrams corresponding to the stable layers and moisture categories described in text and Fig. 12 for four ISS sites.

ing in the dry air). The net effect is to induce a stable layer across the base of the dry intrusion. Relatively sharp temperature inversions can be created in a very dry layer in a period as short as a day. MZ96 speculate that "melting convergence" in COARE mesoscale convective systems (Fig. 11a of Mapes and Houze 1995) may draw dry air from the subtropics over the warm pool near the melting level (supported by Fig. 18), which is then radiatively stabilized on the timescale of a day. TOGA COARE sounding-based divergence profiles (Lin and Johnson 1996) do not show sharp melting-layer convergence because they average over very large areas that include convection and its environment. Dense sounding networks in the environment of convection do, however, exhibit shallow layers of strong convergence into convective systems at the melting level (e.g., Johnson et al. 1995).

There is also evidence to indicate that the warm–dry perturbations above the 0°C level may reflect the presence of convectively generated gravity waves, although their net effect is uncertain due to transience, mean flow effects, and other factors. In particular, heat sources resembling those associated with tropical cloud clusters generate internal gravity waves (Szeto et al. 1988; Nicholls et al. 1991), referred to by Mapes (1993) as "buoyancy bores." The net effect of these bores can be to increase stability at midlevels (Nicholls et al. 1991). An example of the impact on the temperature field is shown in Fig. 19 (from Mapes and Houze 1995), a depiction of the simulated temperature perturbation six hours after the initiation of an imposed heat source characterized by the divergence profile measured by aircraft Doppler radar withing COARE mesoscale convective systems. A sharp layer of warming within 500 km of the heat source (assumed to have a ~75 km radius) can be seen at and above 6 km (just above the 0°C level). This warming is a consequence of deep tropospheric subsidence associated with a 50 m s^{-1} bore augmented above 6 km and entirely counteracted at low levels by adiabatic cooling associated with a 25 m s^{-1} bore. The subsidence aloft could also explain the concurrent drying that is observed. However, many of the dry layers are too sharp and too dry to be explained by this mecha-

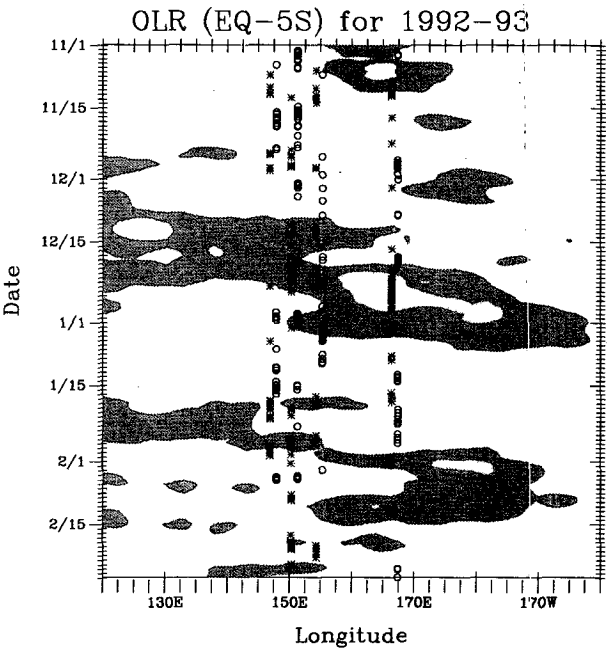

FIG. 15. Hovmöller diagram for COARE IOP of OLR (with values below 190 W m^{-2} indicated with dark shading and values below 150 W m^{-2} indicated with lighter shading). Also plotted are the occurrences of stable layers from the driest (RH− −) and moistest categories (RH++, described in text and Fig. 12), indicated by the circles and asterisks, respectively. The symbols for the dry (moist) cases are offset slightly to the right (left) of the longitudes of the four sites: Manus (147.3°E), Kavieng (150.8°E), Kapinga (154.8°E), and Nauru (166.9°E). No occurrences are plotted for Manus from 1 December to 23 December 1992 due to bad humidity data at this site during this period.

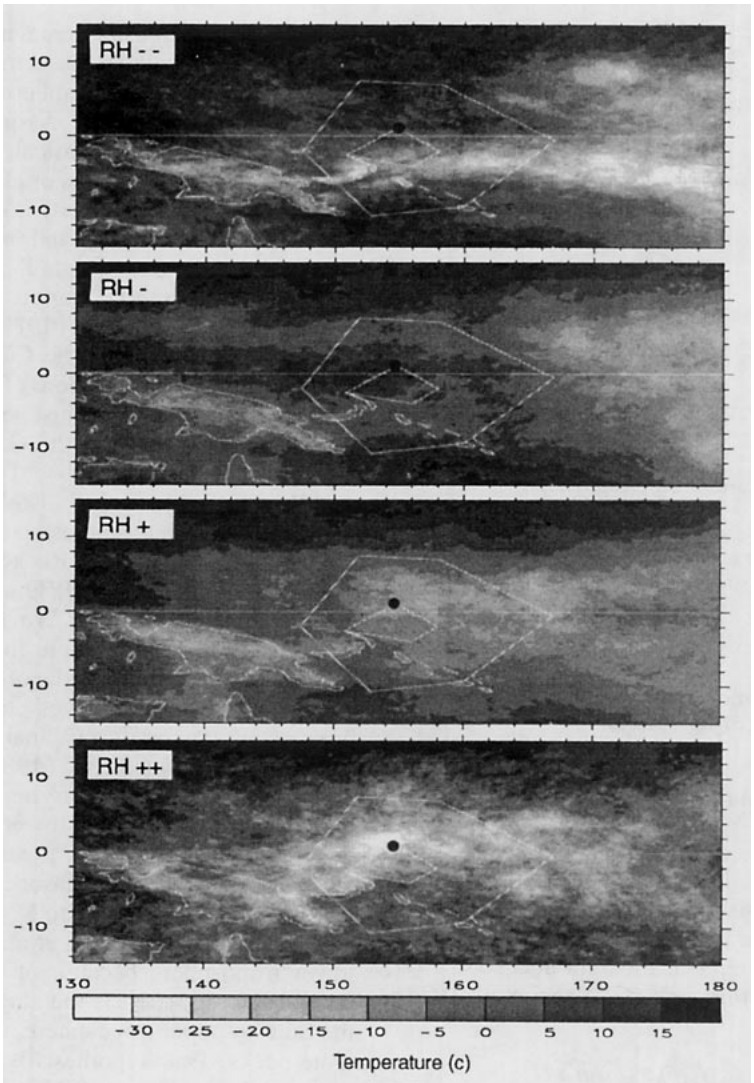

FIG. 16. Composite IR brightness maps corresponding to the occurrences of stable layers at Kapinga (location indicated by black dot) for each of the moisture categories described in text and Fig. 12.

nism alone. Mapes and Houze (1995) also find that the shallow layer of convergence observed near the melting level within convective systems excites a slow-moving mode with shallow vertical structure that could explain the particularly sharp temperature perturbations that we are finding. The layered vertical structure of T' for the RH− category (Fig. 12b) resembles the "melting-layer reverberation," warm–cool–warm pattern, for this slow-moving mode described by Mapes and Houze (1995) and seen near the origin in Fig. 19.

Another possible mechanism for the stable layers involves balanced theory and potential vorticity (PV) inversion. In this explanation the cooling associated with melting, when combined with condensation heating aloft and evaporative cooling below, produces a strong vertical gradient in the diabatic heating rate (i.e., $\dot{\theta}$). Mass is removed from the isentropic layers near the melting level, thereby creating a local positive PV anomaly (e.g., Raymond and Jiang 1990). When this anomaly is inverted to obtain the associated balanced wind and mass fields, a horizontal spreading effect occurs, resulting in a temperature inversion in regions horizontally distant from the melting. Preliminary results from computations using methods similar to those employed in Schubert et al. (1995), involving observed melting-induced cooling profiles within two relatively narrow zonal ITCZ bands at 10°N and S, show that after three days there is a remote effect in the cloud-free region

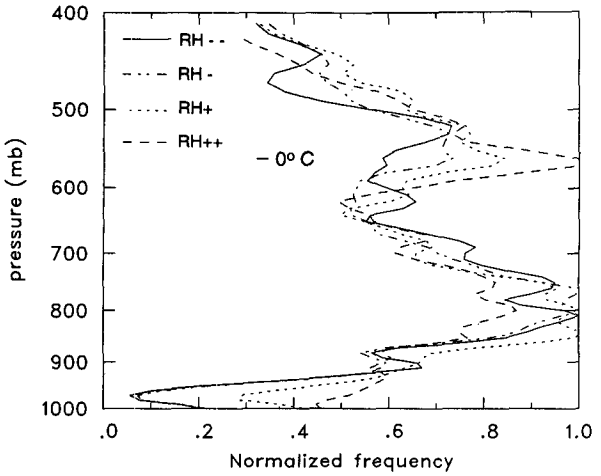

FIG. 17. Cumulative frequency (percent) of temperature lapse rates less than 5°C km^{-1} for four relative humidity categories, with each curve normalized by its maximum value in the 1000–400-mb layer for four ISS sites.

along the equator, namely, an increase in stability of 1.5°C km^{-1} near the 0°C level.

6. Impacts on vertical distributions of heating and moistening

In a global context, there is considerable evidence based on heat and moisture budget studies for the existence of perturbations in the temperature and moisture fields near the 0°C level. The apparent heat source Q_1, and the apparent moisture sink Q_2 (Yanai et al. 1973), can be defined by

$$Q_1 \equiv c_p\left[\frac{\partial \bar{T}}{\partial t} + \bar{\mathbf{v}}\cdot\nabla\bar{T} + \left(\frac{p}{p_0}\right)^{\kappa}\bar{\omega}\frac{\partial\bar{\theta}}{\partial p}\right]$$
$$= Q_R + L_v(\bar{c}-\bar{e}) + (L_v+L_f)(\bar{d}-\bar{s}_*) + L_f(\bar{f}-\bar{m}) - \frac{\partial}{\partial p}\overline{\theta'\omega'} \quad (1)$$

$$Q_2 \equiv -L_v\left[\frac{\partial\bar{q}}{\partial t} + \bar{\mathbf{v}}\cdot\nabla\bar{q} + \bar{\omega}\frac{\partial\bar{q}}{\partial p}\right]$$
$$= L_v(\bar{c}-\bar{e}) + L_v(\bar{d}-\bar{s}_*) + L_v\frac{\partial}{\partial p}\overline{q'\omega'}, \quad (2)$$

where c, e, d, s_*, f, and m are condensation, evaporation, deposition, sublimation, freezing, and melting rates, respectively; θ is potential temperature; $\mathbf{v}$ horizontal wind; $\omega = dp/dt$; Q_R radiative heating rate; $\kappa = R/c_p$; R and c_p gas constant and the specific heat at constant pressure of dry air, respectively; L_v and L_f the latent heats of vaporization and fusion, $p_0 = 1000$ hPa; overbar refers to a horizontal average; and prime refers to a deviation from this average.

In the Tropics, the horizontal and temporal variations of q and T are small, so the vertical advection terms in (1) and (2) are the dominant contributors to Q_1 and Q_2 in convective situations. Assuming $\bar{\omega}$ is a single-peaked function in the vertical, profiles of Q_1 and Q_2 should reflect perturbations or inflections in the vertical profiles of q and T near the 0°C level (Figs. 3b and 3d) since they contain $\partial\bar{q}/\partial p$ and $\partial\bar{\theta}/\partial p$. Plots of Q_2 normalized by precipitation rate P_0, that is, Q_2/P_0, for the eastern Atlantic GATE region [easterly wave trough data from Thompson et al. (1979)], the western Pacific (Yanai et al. 1973) and the COARE OSA region indeed show these perturbations (Fig. 20). In each region there is a minimum in Q_2 just below the 0°C level (this level is slightly lower in the GATE region where the 0°C level is around 600 mb).[6] This prominent "double peak" structure in Q_2 has also been reported in many other observational studies, both in the Tropics and midlatitudes (Reed and Recker 1971; Lewis 1975; Johnson 1976; Nitta 1977; Frank and McBride 1989; Gallus and Johnson 1991; Wu 1993).

The double-peak structure in Q_2 may also be interpreted by referring to the rhs of (2) or another form of the rhs of (2) that involves cloud detrainment, mass fluxes, and evaporation (Yanai et al. 1973). Johnson (1984) and Esbensen et al. (1988) argued that the double peak arises from the drying effects of two distinct features: deep convective towers, providing the lower-level peak, and stratiform precipitation, providing the upper-level peak. It was reasoned that the cumulus drying, which is proportional to $M_c\partial\bar{q}/\partial p$ [where M_c is the cumulus mass flux, Yanai et al. (1973)], peaks in the lower troposphere because of the exponential (in p) structure to $\bar{q}$, whereas the stratiform drying peaks in the mid- to upper troposphere, thereby giving two separate peaks. This hypothesis is supported to some degree by the results of a 24-h GATE cloud ensemble simulation by Soong and Tao (1980). However, from the perspective of the lhs of (2), this interpretation can only be correct if convective and stratiform components produce a double peak in $\bar{\omega}$ or cause an inflection in the $\bar{q}$ profile (so that $\partial\bar{q}/\partial p$ has a double peak). On the other hand, Dudhia and Moncrieff (1987), Lafore et al. (1988), and Chong and Hauser (1990) have proposed using cloud-modeling studies that the vertical eddy transport of water vapor [rhs of (2)] influences the Q_2 profiles and in some instances can actually account for the double-peak structure. However, Dudhia and Moncrieff note that this interpretation in their case arises from a reversal in the mean vertical moisture

[6] Unlike the OSA-mean Q_2 profile, the IFA-mean (not shown) does not exhibit a minimum near the 0°C level when averaged for the entire IOP. It does, however, during periods of deep convection. During periods of strong westerlies, enhanced subsidence and the existence of many shallow cumulus lead to prolonged periods of negative Q_2 (moistening), which significantly affects the IOP-mean Q_2 profile.

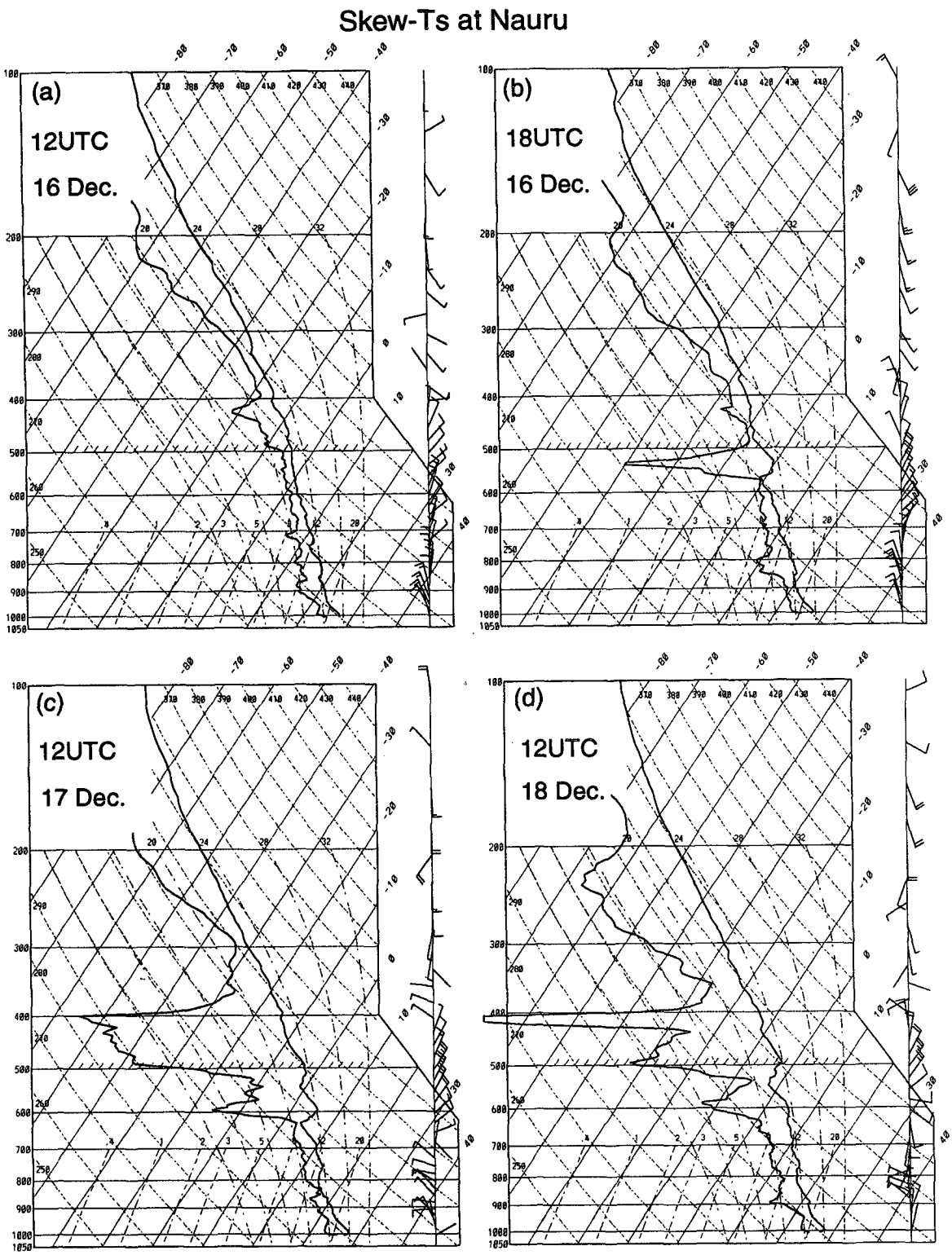

FIG. 18. Skew T diagrams for Nauru at (a) 1200 UTC 16 December, (b) 1800 UTC 16 December, (c) 1200 UTC 17 December, and (d) 1200 UTC 18 December 1992 depicting a sequence of soundings from a 2-day period that was characterized by a sudden onset of dry, stable layers near the 0°C level with associated acceleration of the northeasterly flow, suggesting dry intrusions from the subtropics.

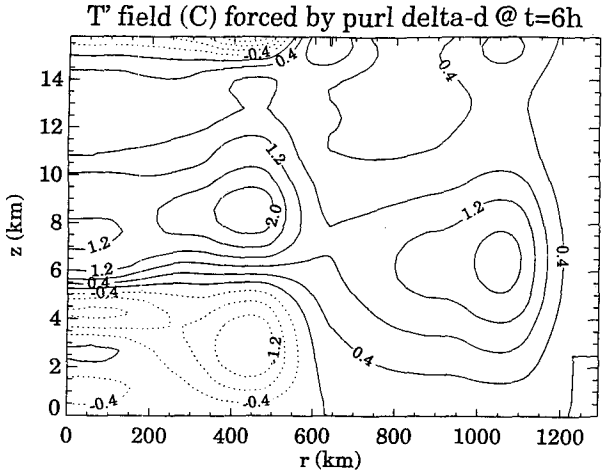

FIG. 19. Simulated temperature perturbation field six hours after the initiation of an imposed heat source characterized by the divergence profile measured by aircraft Doppler radar within COARE mesoscale convective systems (from Mapes and Houze 1995).

gradient in the sounding used to initialize the model. Similar effects from initial soundings can be seen in the other studies.

Regardless of interpretation, the lhs of (2) makes it clear that the often-observed double-peak structure to Q_2 can be attributed to frequently occurring reversals or inflections in the q profile. The question then follows: why do reversals or inflections occur in the q profile? One possibility, implicit in the Johnson (1984) and Esbensen et al. (1988) hypothesis, is that the upper-level stratiform cloud systems cover significant areas (Houze 1977, 1982; Zipser 1977; Cheng and Houze 1979) and therefore impact the vertical moisture distribution. These clouds typically have their bases near the 0°C level (Leary and Houze 1979) in part due to cooling by melting, which induces a downward acceleration below that level (Lord et al. 1984). The moist conditions at and above the 0°C level could then be a consequence of the common occurrence of stratiform precipitation systems; however, how they might act to perturb the mean q profile to yield a moist anomaly in a ~50-mb layer centered about 0°C (implied from $\partial\bar{q}/\partial p$ profile in Fig. 3d) is not completely clear. Another possibility is that enhanced detrainment from cumulonimbus occurs near 0°C because of the increased stability there (Bretherton and Smolarkiewicz 1989). This detrainment could lead to enhanced cloud layers or shelf clouds (hence moistening) near the 0°C level, which are suggested in the RH analyses of MZ96 (their Fig. 18) and in recent space shuttle lidar data (M. Platt 1995, personal communication).

Due to the high frequency of stable layers near the 0°C level, one might expect profiles of Q_1 to reflect their presence, as mentioned earlier. However, the impact is far less than on Q_2, as shown in Fig. 21. Only slight inflections are evident between 600 and 700 mb. The explanation for the difference is that while Q_2 is proportional to $\bar{w}\partial\bar{q}/\partial z$, Q_1 is proportional to $\bar{w}(\partial\bar{T}/\partial z + g/c_p)$. The adiabatic term g/c_p is large and perturbations to the $\bar{T}$ profile (Fig. 3a) only have a minor net effect on Q_1. It is also evident from Fig. 21 that cooling effects due to melting [$-L_f\bar{m}$ in (1)] are small relative to the net heating by condensation and deposition when averaged over the convective and stratiform components of many cloud systems. However, for at least one mesoscale convective system during COARE a pronounced notch in the Q_1 profile has been detected at 0°C and attributed to highly localized cooling due to melting within the stratiform region (Carey et al. 1994).

7. Impacts of stable layers on convection and cloudiness

Once stable layers are produced, regardless of the mechanism(s), there are potential impacts on subsequent convection and the distribution of moisture. One possibility is that deep convection penetrating the stable layers could lead to enhanced detrainment and moistening near that level (Bretherton and Smolarkiewicz 1989; Taylor and Baker 1991; Raymond and Blyth 1992). The peak in "cloudy layers" near the 0°C level determined by MZ96 from RH data supports this idea. Similar midlevel cloud layers have been observed on trans-Pacific aircraft flights by Malkus and Riehl

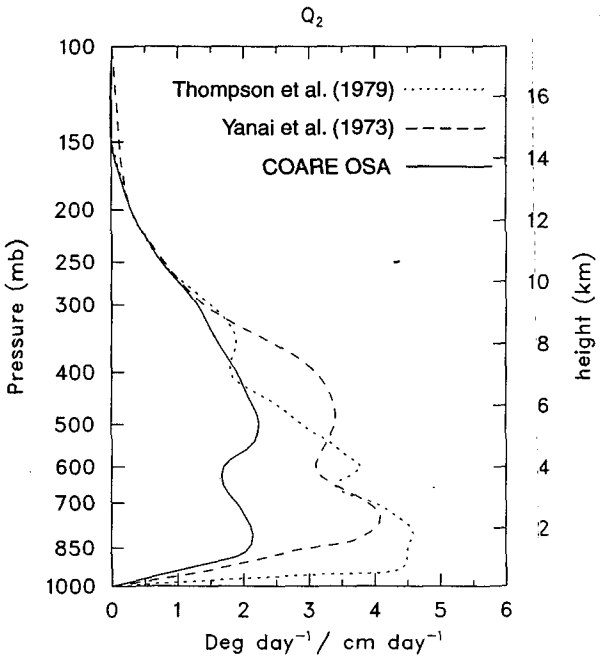

FIG. 20. Normalized apparent moisture sink (Q_2) for the East Atlantic (Thompson et al. 1979), for the Marshall Islands region of the West Pacific (Yanai et al. 1973), and for the COARE OSA.

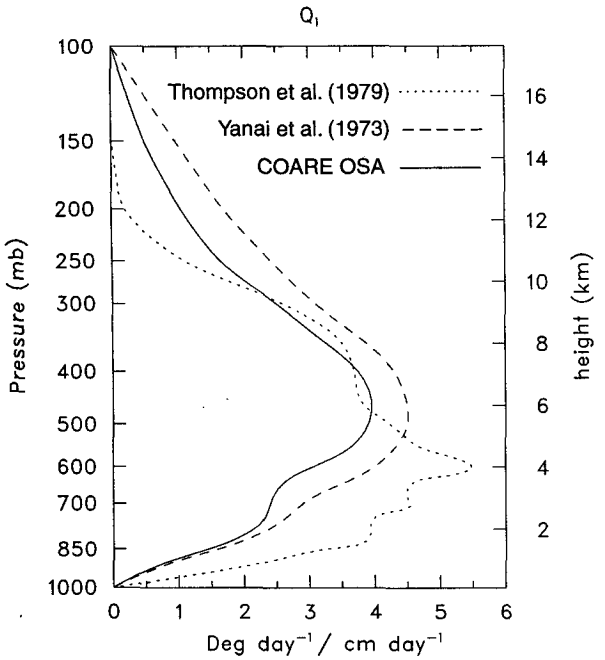

FIG. 21. Normalized apparent heat source (Q_1) for the East Atlantic (Thompson et al. 1979), for the Marshall Islands region of the West Pacific (Yanai et al. 1973), and for the COARE OSA.

(1964), in the eastern Atlantic (Thompson et al. 1979), in the vicinity of hurricanes (F. Marks 1995, personal communication), and in recent space shuttle lidar measurements over the western Pacific (M. Platt 1995, personal communication).

Mapes and Zuidema (1996) show that stable layers near 0°C, while not strong enough to totally negate the buoyancy of a penetrating cloud, can promote enhanced detrainment near the melting level and partly retard cloud growth. Possible evidence of this effect can be seen in TOGA COARE Doppler radar observations from Manus (Uyeda et al. 1995) where during the mature stage of convective systems a secondary maximum in radar reflectivity was reported above the melting layer (the primary maximum being below the melting layer) with a minimum at 0°C. Similarly, Cifelli and Rutledge (1994) found a double-peaked vertical velocity profile in Australian monsoon convection with a minimum in ω near 0°C. There is also a suggestion from TOGA COARE data from the MIT radar aboard the R/V *Vickers* (Rickenbach 1995) of a bimodal population of precipitating clouds at several times during the IOP, with one peak near the tropopause and another in the midtroposphere. Similar peaks in midlevel echo tops were reported in GATE (Cheng and Houze 1979). Although MZ96 show that stable layers near 0°C likely do not significantly affect the ultimate heights of deep, nonentraining cumulonimbi, they may affect the growth of entraining, precipitation-laden congestus—thereby possibly producing a bimodal population of precipitating clouds. This conjecture, of course, awaits testing by cloud models. If cloud growth is restricted to beneath the 0°C level and just above, it limits the role freezing can play in promoting growth to yet higher levels.

8. Summary and conclusions

Sounding data from TOGA COARE reveal the common occurrence of stable layers near the trade wind (800 mb or 2 km) level and the 0°C level over the western Pacific warm pool. For a stability threshold of -5 C km^{-1}, roughly 50% (80%) of the soundings contain trade wind stable layers, assuming these stable layers are within 10 mb (50 mb) of 800 mb, and approximately one-half exhibit stable layers near the 0°C level. Many of the soundings in the latter group appear to be associated with the direct effects of melting in tropical convective systems, characterized by cooling in a ~500 m layer just below 0°C. Once generated, these melting-induced stable layers may persist for a day or longer until destroyed by vertical mixing, radiation, or subsequent convection. However, many stable layers occurred in extremely dry environments, suggesting other explanations are needed for their existence. The finding of ubiquitous trade wind stable layers over the warm pool, though not widely recognized, is consistent with the frequent observations of trade cumulus throughout the TOGA COARE domain. These trade inversions often coexist with, but are distinct from, the inversions near the 0°C level.

The sounding data were stratified according to values of midtropospheric relative humidity. Of four categories defined, ranging from very moist to very dry, stable layers near the 0°C level fell into two main classifications: anomalously cool–moist conditions at and slightly below the 0°C level and anomalously warm–dry conditions at and just above. The former occurred primarily within or in close proximity to precipitating systems, suggesting they are primarily a direct result of melting within stratiform rain areas. Soundings in the latter group typically occurred outside convective areas. Mechanisms for their formation are unclear at this time, but advective, radiative, gravity wave, and melting effects may all play some role. One possibility consistent with our observations is radiative stabilization of "dry tongues" (MZ96). Shallow, dry layers may be preferentially drawn over the warm pool from the dry subtropics by strong convergence near the melting level in equatorial convection.

The perturbation in the specific humidity profile, which is amplified when its vertical derivative is taken, explains the frequently observed double-peak structure to the apparent moisture sink Q_2 in the Tropics. While temperature perturbations might also be expected to produce a similar double-peak structure to the apparent heat source Q_1, it is normally not observed because the effect is mitigated by a larger term involving g/c_p.

Congestus impinging upon and/or deep cumulonimbus penetrating the stable layers may account for the moisture perturbations or inflections in the q profile near the 0°C level through enhanced detrainment (Bretherton and Smolarkiewicz 1989). This detrainment may explain the shelf clouds frequently seen attached to tropical cumulonimbi. The existence of such clouds is supported by MZ96 inference of a maximum in "cloudy layers" near 0°C based on relative humidity observations.

Several areas of research are suggested by these observations. First, the geographical distributions of the stable layers described in this paper need further investigation. Already we have indicated that stable layers near 0°C exist over the Atlantic and eastern Pacific; however, their frequency, horizontal distribution, and relationship to moisture perturbations are not well known. Second, possible impacts on tropical cumulus cloud populations are suggested by some tropical radar observations, but results so far are inconclusive. Finally, considerable research is needed on mechanisms for the temperature and moisture perturbations. As speculated, many processes may be involved, singly or coupled. Further analysis of the COARE observations may shed light on these mechanisms.

Acknowledgments. We thank Brian Mapes for his careful review of the paper and many discussions on this topic. Appreciation is also extended to Robert Fovell for his valuable comments concerning statistical analyses undertaken to determine the dominant modes of variability of the temperature and moisture profiles in an earlier version of this work. In addition, we thank Xin Lin and Jim Bresch for their considerable contributions to data analysis and to Wayne Schubert, Bob Houze, and Dave Gutzler for their valuable comments. Special appreciation is extended to Roger Lukas and Peter Webster for their exceptional efforts in conceiving, planning, and implementing TOGA COARE. This research has been supported by the National Oceanic and Atmospheric Administration under Grants NA90RAH00077 and NA37RJ0202.

REFERENCES

Ananthakrishnan, R., and R. N. Keshvamurthy, 1974: Some new features of the vertical distribution of temperature and humidity over Bombay during the southwest monsoon season. *J. Mar. Biol. Assoc. India,* **14**(2), 732–742.

Atlas, D., R. Tatehira, R. C. Srivastava, W. Marker, and R. E. Carbone, 1969: Precipitation-induced mesoscale wind perturbations in the melting layer. *Quart. J. Roy. Meteor. Soc.*, **95,** 544–560.

Augstein, E., H. Schmidt, and F. Ostapoff, 1974: The vertical structure of the atmospheric planetary boundary layer in undisturbed trade winds over the Atlantic Ocean. *Bound.-Layer. Meteor.*, **6,** 129–149.

Betts, A. K., and B. A. Albrecht, 1987: Conserved variable analysis of the convective boundary layer thermodynamic structure over the tropical oceans. *J. Atmos. Sci.*, **44,** 83–99.

Bretherton, C. S., and P. K. Smolarkiewicz, 1989: Gravity waves, compensating subsidence and detrainment around cumulus clouds. *J. Atmos. Sci.*, **46,** 740–759.

Carey, L. D., S. A. Rutledge, and R. H. Johnson, 1994: Heat and moisture budget over the TOGA COARE IFA during the mature phase of the 24 December mesoscale convective system. Preprints, *Sixth Conf. on Mesoscale Processes,* Portland, OR, Amer. Meteor. Soc., 5–8.

Chen, S. S., R. A. Houze Jr., and B. E. Mapes, 1996: Multiscale variability of deep convection in relation to large-scale circulation during TOGA COARE. *J. Atmos. Sci.*, **53,** 1380–1409.

Cheng, C.-P., and R. A. Houze, Jr., 1979: The distribution of convective and mesoscale precipitation in GATE radar echo patterns. *Mon. Wea. Rev.*, **107,** 1370–1381.

Chong, M., and D. Hauser, 1990: Tropical squall line observed during the COPT 81 experiment in West Africa. *Mon. Wea. Rev.*, **118,** 1696–1706.

Cifelli, R., and S. A. Rutledge, 1994: Vertical motion structure in maritime continent mesoscale convective systems: Results from a 50-MHz profiler. *J. Atmos. Sci.*, **51,** 2631–2652.

Dudhia, J., and M. W. Moncrieff, 1987: A numerical simulation of quasi-stationary tropical convective bands. *Quart. J. Roy. Meteor. Soc.*, **113,** 929–967.

Esbensen, S. K., J.-T. Wang, and E. I. Tollerud, 1988: A composite life cycle of nonsquall mesoscale convective systems over the tropical ocean. Part II: Heat and moisture budgets. *J. Atmos. Sci.*, **45,** 537–548.

Findeisen, W., 1940: The formation of the 0°C isothermal layer and fractocumulus under nimbostratus. *Meteorol. Z.*, **57,** 49–54.

Firestone, J. K., and B. A. Albrecht, 1986: The structure of the atmospheric boundary layer in the central equatorial Pacific during January and February of FGGE. *Mon. Wea. Rev.*, **114,** 2219–2231.

Frank, W. M., and J. L. McBride, 1989: The vertical distribution of heating in AMEX and GATE cloud clusters. *J. Atmos. Sci.*, **46,** 3464–3478.

Gage, K. S., C. R. Williams, and W. L. Ecklund, 1994: UHF wind profilers: A new tool for diagnosing tropical convective cloud systems. *Bull. Amer. Meteor. Soc.*, **75,** 2289–2294.

Gallus, W. A., Jr., and R. H. Johnson, 1991: Heat and moisture budgets of an intense midlatitude squall line. *J. Atmos. Sci.*, **48,** 122–146.

Gutnick, M., 1958: Climatology of the trade-wind inversion in the Caribbean. *Bull. Amer. Meteor. Soc.*, **39,** 410–420.

Gutzler, D. S., 1993: Uncertainties in climatological tropical humidity profiles: Some implications for estimating the greenhouse effect. *J. Climate,* **6,** 978–982.

——, G. N. Kiladis, G. A. Meehl, K. M. Weickmann, and M. Wheeler, 1994: The global climate of December 1992–February 1993. Part II: Large-scale variability across the tropical western Pacific during TOGA COARE. *J. Climate,* **7,** 1606–1622.

Haraguchi, P. Y., 1968: Inversions over the tropical eastern Pacific Ocean. *Mon. Wea. Rev.*, **96,** 177–185.

Hendon, H. H., and B. Liebmann, 1990: The intraseasonal (30–50-day) oscillation of the Australian summer monsoon. *J. Atmos. Sci.*, **47,** 2909–2923.

Houze, R. A., Jr., 1977: Structure and dynamics of a tropical squall-line system. *Mon. Wea. Rev.*, **105,** 1540–1567.

——, 1982: Cloud clusters and large-scale vertical motion in the tropics. *J. Meteor. Soc. Japan,* **60,** 396–410.

Johnson, R. H., 1976: The role of convective-scale precipitation downdrafts in cumulus and synoptic-scale interactions. *J. Atmos. Sci.*, **33,** 1890–1910.

——, 1984: Partitioning tropical heat and moisture budgets into cumulus and mesoscale components: Implications for cumulus parameterization. *Mon. Wea. Rev.*, **112,** 1590–1601.

——, B. D. Miner, and P. E. Ciesielski, 1995: Circulations between mesoscale convective systems along a cold front. *Mon. Wea. Rev.*, **123,** 585–599.

Jordan, C. L., 1958: Mean soundings for the West Indies area. *J. Meteor.*, **15,** 91–97.

Kloesel, K. A., and B. A. Albrecht, 1989: Low-level inversions over the tropical Pacific—Thermodynamic structure of the boundary

layer and above-inversion moisture structure. *Mon. Wea. Rev.*, **117,** 87–101.

Lafore, J.-P., J.-L. Redelsperger, and G. Jaubert, 1988: Comparison between a three-dimensional simulation and Doppler radar data of a tropical squall line: Transports of mass, momentum, heat and moisture. *J. Atmos. Sci.*, **45,** 3483–3500.

Leary, C. A., and R. A. Houze, Jr., 1979: Melting and evaporation of hydrometeors in precipitation from the anvil clouds of deep tropical convection. *J. Atmos. Sci.*, **36,** 669–679.

Lewis, J. M., 1975: Test of the Ogura-Cho model on prefrontal squall line case. *Mon. Wea. Rev.*, **103,** 764–778.

Lin, X., and R. H. Johnson, 1996: Kinematic and thermodynamic characteristics of the flow over the western Pacific warm pool during TOGA COARE. *J. Atmos. Sci.*, **53,** 695–715.

Liu, W. T., W. Tang, and P. P. Niiler, 1991: Humidity profiles over the ocean. *J. Climate,* **4,** 1023–1034.

Lord, S. J., H. E. Willoughby, and J. M. Piotrowicz, 1984: Role of parameterized ice-phase microphysics in an axisymmetric, nonhydrostatic tropical cyclone model. *J. Atmos. Sci.*, **41,** 2836–2848.

Malkus, J. S., and H. Riehl, 1964: *Cloud Structure and Distributions over the Tropical Pacific Ocean.* University of California Press, 229 pp.

Mapes, B. E., 1993: Gregarious tropical convection. *J. Atmos. Sci.*, **50,** 2026–2037.

——, and R. A. Houze Jr., 1992: An integrated view of the 1987 Australian monsoon and its mesoscale convective systems. I: Horizontal structure. *Quart. J. Roy. Meteor. Soc.*, **118,** 927–963.

——, and ——, 1995: Diabatic divergence profiles in western Pacific mesoscale convective systems. *J. Atmos. Sci.*, **52,** 1807–1828.

——, and P. Zuidema, 1996: Radiative-dynamical consequences of dry tongues in the tropical atmosphere. *J. Atmos. Sci.*, **53,** 620–638.

Miller, E., 1993: TOGA COARE dropsonde data report. National Center for Atmospheric Research, 75 pp. [Available from Surface and Sounding Systems Facility, National Center for Atmospheric Research, Boulder, CO 80307-3000.]

Nakazawa, T., 1995: Intraseasonal oscillations during the TOGA-COARE IOP. *J. Meteor. Soc. Japan,* **73,** 305–319.

Nicholls, M. E., R. A. Pielke, and W. R. Cotton, 1991: Thermally forced gravity waves in an atmosphere at rest. *J. Atmos. Sci.*, **48,** 1869–1884.

Nitta, T., 1977: Response of cumulus updraft and downdraft to GATE A/B-scale motion systems. *J. Atmos. Sci.*, **34,** 1163–1186.

Numaguti, A., R. Oki, K. Nakamura, K. Tsuboki, N. Misawa, T. Asai, and Y.-M. Kodama, 1995: 4–5-day-period variations and low-level dry air observed in the equatorial western Pacific during the TOGA-COARE IOP. *J. Meteor. Soc. Japan,* **73,** 267–290.

Parsons, D., W. Dabberdt, H. Cole, T. Hock, C. Martin, A.-L. Barrett, E. Miller, M. Spowart, M. Howard, W. Ecklund, D. Carter, K. Gage, and J. Wilson, 1994: The integrated sounding system: Description and preliminary observations from TOGA COARE. *Bull. Amer. Meteor. Soc.*, **75,** 553–567.

Randall, D. A., Harshvardan, and D. A. Dazlich, 1991: Diurnal variability of the hydrological cycle in a general circulation model. *J. Atmos. Sci.*, **48,** 40–62.

Raymond, D. J., and H. Jiang, 1990: A theory for long-lived mesoscale convective systems. *J. Atmos. Sci.*, **47,** 3067–3077.

——, and A. M. Blyth, 1992: Extension of the stochastic mixing model to cumulonimbus clouds. *J. Atmos. Sci.*, **49,** 1968–1983.

Reed, R. J., and E. E. Recker, 1971: Structure and properties of synoptic-scale wave disturbances in the equatorial western Pacific. *J. Atmos. Sci.*, **28,** 1117–1133.

Rickenbach, T. M., 1995: Rainfall production from the spectrum of convection observed by shipboard radar during TOGA COARE. Preprints, *21st Conf. on Hurricanes and Tropical Meteorology,* Miami, FL, Amer. Meteor. Soc., 116–118.

Riehl, H., 1977: Venezuelan rain systems and the general circulation of the summer tropics: Rain systems. *Mon. Wea. Rev.*, **105,** 1402–1420.

Schubert, W. H., P. E. Ciesielski, C. Lu, and R. H. Johnson, 1995: Dynamical adjustment of the trade wind inversion layer. *J. Atmos. Sci.*, **52,** 2941–2952.

Soong, S.-T., and W.-K. Tao, 1980: Response of deep tropical clouds to mesoscale processes. *J. Atmos. Sci.*, **37,** 2016–2034.

Stewart, R. E., J. D. Marwitz, J. C. Pace, and R. E. Carbone, 1984: Characteristics through the melting layer of stratiform clouds. *J. Atmos. Sci.*, **41,** 3227–3237.

Sun, D.-Z., and R. S. Lindzen, 1993: Distribution of tropical tropospheric water vapor. *J. Atmos. Sci.*, **50,** 1643–1660.

Szeto, K. K., C. A. Lin, and R. E. Stewart, 1988: Mesoscale circulations forced by melting snow. Part I: Basic simulations and dynamics. *J. Atmos. Sci.*, **45,** 1629–1641.

Taylor, G. R., and M. B. Baker, 1991: Entrainment and detrainment in cumulus clouds. *J. Atmos. Sci.*, **48,** 112–121.

Thompson, R. M., Jr., S. W. Payne, E. E. Recker, and R. J. Reed, 1979: Structure and properties of synoptic-scale wave disturbances in the intertropical convergence zone of the eastern Atlantic. *J. Atmos. Sci.*, **36,** 53–72.

Uyeda, H., and Coauthors, 1995: Doppler radar observations on the structure and characteristics of tropical clouds during the TOGA-COARE IOP in Manus, Papua New Guinea—outline of the observation. *J. Meteor. Soc. Japan,* **73,** 415–425.

Webster, P. J., and R. Lukas, 1992: TOGA COARE: The Coupled Ocean–Atmosphere Response Experiment. *Bull. Amer. Meteor. Soc.*, **73,** 1377–1416.

Wexler, R., R. Reed, and J. Honing, 1954: Atmospheric cooling by melting snow. *Bull. Amer. Meteor. Soc.*, **35,** 48–51.

Williams, C. R., W. L. Ecklund, and K. S. Gage, 1995: Classification of precipitating clouds in the tropics using 915-MHz wind profilers. *J. Atmos. Oceanic Technol.*, **12,** 996–1012.

Willis, P. T., and A. J. Heymsfield, 1989: Structure of the melting layer in mesoscale convective system stratiform precipitation. *J. Atmos. Sci.*, **46,** 2008–2025.

Wu, X., 1993: Effects of cumulus ensemble and mesoscale stratiform clouds in midlatitude convective systems. *J. Atmos. Sci.*, **50,** 2496–2518.

Yanai, M., S. Esbensen, and J. H. Chu, 1973: Determination of bulk properties of tropical cloud clusters from large-scale heat and moisture budgets. *J. Atmos. Sci.*, **30,** 611–627.

Yoneyama, K., and T. Fujitani, 1995: The behavior of dry westerly air associated with convection observed during TOGA-COARE R/V *Natsushima* cruise. *J. Meteor. Soc. Japan,* **73,** 291–304.

Yuter, S. E., and R. A. Houze Jr., 1995: Three-dimensional kinematic and microphysical evolution of Florida cumulonimbus. Part II: Frequency distributions of vertical velocity, reflectivity, and differential reflectivity. *Mon. Wea. Rev.*, **123,** 1941–1963.

Zipser, E. J., 1977: Mesoscale and convective-scale downdrafts as distinct components of squall-line circulation. *Mon. Wea. Rev.*, **105,** 1568–1589.